T_c Enhancement Induced by Quantum Ionic Vibrations in Compressed Stannane of $P6_3/mmc$ Phase

Mi Pang(庞蜜)[1], Pugeng Hou(侯朴赓)[2*], Mingqi Li(李明奇)[1], Wenjia Shi(史文佳)[1], and Yao Ma(马遥)[1*]

[1]*School of Optoelectronic Science and Intelligent Instrumentation & Shaanxi University Key Laboratory of Photonic Power Devices and Discharge Regulation, Xi'an University of Technology, Xi'an 710048, China*
[2]*College of Science, Northeast Electric Power University, Jilin 132012, China*

(Received 15 December 2025; accepted manuscript online 2 February 2026)

High-pressure hydrides have emerged as promising superconducting materials, attracting considerable attention in recent years. In this work, by combining the stochastic self-consistent harmonic approximation with first-principles calculations, we elucidate crucial corrections to the vibrational and superconducting properties arising from quantum and anharmonic ionic vibrations of SnH_4 in $P6_3/mmc$ phase at 150–240 GPa. Compared with the classical harmonic approximation, inclusion of these effects results in a pronounced softening (over 500 cm^{-1}) of hydrogen-derived optical phonon modes, and increases the superconducting critical temperature (T_c) from 65 K to 79 K ($\mu^* = 0.1$; isotropic Migdal–Eliashberg theory), corresponding to a 22% enhancement. For $\mu^* = 0.13$, the predicted T_c is approximately 70 K. Analysis of the Eliashberg spectral function confirms that hydrogen vibrational modes constitute the dominant tuning mechanism. These results provide quantitative insights into quantum ionic effects in hydride superconductors.

DOI: 10.1088/0256-307X/43/3/030714 CSTR: 32039.14.0256-307X.43.3.030714

1. Introduction. High-pressure hydrides are among the most intensively investigated classes of superconductors today,[1–23] owing to their relatively high critical temperatures (T_c), which render the prospect of achieving room-temperature superconductors plausible. The idea that hydrogen could exhibit superconductivity was first proposed by Neil Ashcroft in 1968,[24] sparking sustained interest owing to its potential for exceptionally high critical temperatures T_c. However, metallization and superconductivity in pure hydrogen require extraordinarily high pressures that remain beyond current experimental capabilities. The rapid development of this field was catalyzed by Ashcroft's subsequent prediction[25] that heavy atoms in hydrogen-rich compounds could induce a "prepressurization" effect, thereby substantially reducing the external pressure required to achieve metallization and superconductivity. Guided by this concept, several hydrides have been identified as high-pressure superconductors with remarkably high T_c values, such as H_3S with a T_c of 203 K at 155 GPa[26] and LaH_{10} with a T_c of 260 K at 180–200 GPa.[27] These findings have generated intense research interest in superconductivity of high-pressure hydrides in recent years.

Significant progress has been made in experimental and theoretical understanding of hydride superconductors. However, the direct connection between their atomic composition and superconducting properties remains elusive. This gap underscores the critical need to expand data accumulation across this field. Among the diverse families of hydrides, binary hydrides constitute a fundamental category, often serving as parent compounds for the synthesis of high-T_c poly-hydrides. Binary hydrides are far more complicated than they seem, with controversies still existing in many of them. The tin hydride system, whose superconducting properties were first investigated in 2007, remains far from being fully understood. In 2007, Tse *et al.* investigated the $P6/mmm$ phase of SnH_4 in the pressure range of 70–160 GPa using first-principles-based simulations and predicted a T_c of 58–74 K.[28] Later in 2010, Gao *et al.* predicted the structure of SnH_4 and filtered out the $Ama2$ phase above 96 GPa and the $P6_3/mmc$ phase above 180 GPa, with a predicted T_c of 15–22 K for $Ama2$ at 120 GPa and 52–62 K for $P6_3/mmc$ at 200 GPa.[29] The theoretical work of Zhang *et al.* in 2016 suggested that another lower-symmetry phase $C2/m$ dominates above 400 GPa with the predicted T_c ranging from 64–74 K at 500 GPa to 95 K at 600 GPa.[30] In the same year, Mahdi *et al.* investigated different atomic compositions of the tin hydride system and filtered out the $I\bar{4}m2$ phase of SnH_8 above 220 GPa with a T_c of 72–81 K at 220 GPa, the $C2/m$ phase of SnH_{12} above 250 GPa with a T_c of 83–93 K at 250 GPa, and the $C2/m$ phase of SnH_{14} above 300 GPa with a T_c of 86–97 K at 300 GPa.[31] For experimental investigations, Hong *et al.* synthesized tin hydride samples with measured T_c of ∼70 K at 200 GPa and identified the structure of $C2/m$-SnH_{12}.[32] However, their proposed structure was later revised as $Fd\bar{3}m$-Sn_8H_{30} based on X-ray diffraction analysis by Troyan *et al.*,[33] who also claimed observation of the cubic phase $Fd\bar{3}m$-Sn_8H_{30} on their own samples, with the measured T_c of 72 K at

*Corresponding authors. Email: pugeng_hou@neepu.edu.cn; mayao@xaut.edu.cn
© 2026 Chinese Physical Society and IOP Publishing Ltd. All rights, including for text and data mining, AI training, and similar technologies, are reserved.

180 GPa.

All the theoretical predictions in the above studies[28–31] were performed using first-principles calculations based on the density functional theory (DFT), in which ions are treated as classical particles via the harmonic approximation. However, recent theoretical advances have implied that ignoring the quantum and anharmonic natures of ionic vibrations in the harmonic approximation would result in significant deviations in predicting the structural and superconducting properties of many hydrides.[34–46] Motivated by the need to accumulate data and assess quantum and anharmonic ionic effects on tin hydride systems, we performed first-principles calculations of the structural and superconducting properties of stannane (SnH_4) in the $P6_3/mmc$ phase at 150–240 GPa. Incorporating the effects of quantum ionic vibrations through the stochastic self-consistent harmonic approximation (SSCHA),[38,40,47–49] our calculations reveal significant corrections that substantially alter T_c predictions. Within the framework of isotropic Migdal–Eliashberg equations, inclusion of quantum and anharmonic effects increases T_c by ∼22% compared with the classical harmonic approximation. For a Coulomb pseudopotential $\mu^* = 0.13$, this yields a T_c of ∼70 K.

2. Methods and Computational Details. Despite their relatively high critical temperatures, high-pressure hydride superconductors are conventional phonon-mediated systems whose superconducting behavior is generally well-captured and predicted using the BCS/Migdal–Eliashberg framework,[50–54] in contrast to unconventionally high-T_c superconductors. The fact that their physics can be described by conventional single-particle models underpins the success of DFT-based first-principles calculations in describing and predicting their superconducting behavior, such as in the commonly cited cases of H_3S,[55] LaH_{10},[34] YH_6,[56] and among many others.[29,36,57–70] Theoretical prediction of superconducting properties in such systems relies on the accurate characterization of ionic vibrations, typically within the density-functional perturbation theory (DFPT) frameworks.[71] Conventionally, ions are treated as classical particles, whereas the total energy of electronic system at fixed ionic configurations is computed via DFT. The combined energy from the electrons and the interionic potential, known as the Born–Oppenheimer energy, is denoted by $V(\boldsymbol{R})$, where $\boldsymbol{R}$ denotes the ionic configuration. $V(\boldsymbol{R})$ is conventionally expanded up to the second order around its minimum configuration $\boldsymbol{R}_0$, known as the harmonic approximation. Diagonalizing the dynamic matrix

$$D^h_{ab} = \frac{1}{\sqrt{M_a M_b}} \frac{\partial^2 V(\boldsymbol{R})}{\partial R_a \partial R_b}\bigg|_{\boldsymbol{R}_0}, \tag{1}$$

gives the frequencies of the vibrational quanta, i.e., the harmonic phonons. a and b are combined indices that identify the Cartesian coordinates of all the ions. M_a and R_a are the mass and position of the atom a.

The harmonic approximation neglects the quantum nuclear motion, omitting effects originating from ionic kinetic energy and the higher-order anharmonic terms in $V(\boldsymbol{R})$. Collectively, these omitted contributions termed quantum and anharmonic effects have recently been recognized as crucial phenomena for predicting the structural and superconducting behaviors of hydride superconductors. This recognition has spurred further development of various computational methods for the explicit incorporation of these effects.[38,47,72–74] The SSCHA framework has been widely applied to predict the ionic vibrational properties that incorporate quantum and anharmonic effects.[34–42] SSCHA is a variational method aimed at minimizing the free energy of the system $F[\rho] = \min_{\tilde{\rho}} \mathcal{F}[\tilde{\rho}]$, derived from the complete quantum Hamiltonian of the ions. The free energy $\mathcal{F}[\tilde{\rho}] = E[\tilde{\rho}] - TS[\tilde{\rho}]$ maintains all the anharmonic terms. $E[\tilde{\rho}] = \langle K + V(\boldsymbol{R})\rangle_{\tilde{\rho}}$ is the total energy, and K is the kinetic energy operator. $\langle O\rangle_{\tilde{\rho}} = \mathrm{Tr}[O\tilde{\rho}]/\mathrm{Tr}[\tilde{\rho}]$ is the quantum average of the operator O taken at the trial density matrix $\tilde{\rho}$ of the system. T is the temperature and $S[\tilde{\rho}]$ is the entropy. The trial density matrix $\tilde{\rho} = \tilde{\rho}_{\boldsymbol{\mathcal{R}},\boldsymbol{\Phi}}$ is constrained in practical implementations to ensure that the probability distribution of the ionic positions is a Gaussian type and centered at the centroid positions $\boldsymbol{\mathcal{R}}$ with a width $\boldsymbol{\Phi}$ determined by the quantum-thermal fluctuations around $\boldsymbol{\mathcal{R}}$. The SSCHA minimizes $\mathcal{F}[\tilde{\rho}_{\boldsymbol{\mathcal{R}},\boldsymbol{\Phi}}]$ as a function of $\boldsymbol{\mathcal{R}}$ and $\boldsymbol{\Phi}$. The free energy minimization is achieved through stochastic Monte Carlo sampling over configuration space with key properties, such as the total energy and forces, computed using standard DFT calculations. Once $\mathcal{F}[\tilde{\rho}_{\boldsymbol{\mathcal{R}},\boldsymbol{\Phi}}]$ reaches its minimum value $\mathcal{F}[\tilde{\rho}_{\boldsymbol{\mathcal{R}}_{\mathrm{eq}}}, \boldsymbol{\Phi}_{\mathrm{eq}}]$, $\boldsymbol{\mathcal{R}}_{\mathrm{eq}}$ and $\boldsymbol{\Phi}_{\mathrm{eq}}$ determine the average ionic positions and the fluctuations around them, respectively. In the static limits,[38,49,75] phonon frequencies can be determined by diagonalizing the free energy Hessian at $\boldsymbol{\mathcal{R}}_{\mathrm{eq}}$,

$$D^F_{ab} = \frac{1}{\sqrt{M_a M_b}} \frac{\partial^2 F}{\partial R_a \partial R_b}\bigg|_{\boldsymbol{\mathcal{R}}_{\mathrm{eq}}}, \tag{2}$$

which is the mass-rescaled second-order derivative of the free energies obtained at $\boldsymbol{\mathcal{R}}_{\mathrm{eq}}$. This is the quantum anharmonic analog to classical harmonic dynamical matrix $\boldsymbol{D}^h$ [Eq. (1)]. Considering the obtained phonons embody the quantum and anharmonic effects of ions, they are termed the anharmonic phonons. Note that the appearance of the negative eigenvalues of $\boldsymbol{D}^F$ or $\boldsymbol{D}^h$ indicates structural instability with or without quantum and anharmonic effects.

Subsequent superconducting properties are evaluated using Migdal–Eliashberg framework using harmonic or anharmonic phonons as inputs for the standard electron–phonon coupling calculations. The Eliashberg spectral function

$$\alpha^2 F(\omega) = \frac{1}{2\pi N(0) N_q} \sum_{\mu \boldsymbol{q}} \frac{\gamma_\mu(\boldsymbol{q})}{\omega_\mu(\boldsymbol{q})} \delta[\omega - \omega_\mu(\boldsymbol{q})] \tag{3}$$

is calculated at both harmonic and anharmonic levels, where $\gamma_\mu(\boldsymbol{q})$ is the phonon linewidth due to the electron–phonon interaction at the wave vector $\boldsymbol{q}$ of the mode μ, where $N(0)$ is the density of states at the Fermi level, N_q is the number of phonon momentum points used for the Brillouin zone sampling, and $\omega_\mu(\boldsymbol{q})$ represents the phonon frequencies obtained by diagonalizing $\boldsymbol{D}^F$ or $\boldsymbol{D}^h$ in the anharmonic or harmonic calculations.

The electron–phonon coupling constant λ and the average logarithmic frequency $\omega_{\log}$ can be obtained directly from $\alpha^2F(\omega)$ because $\lambda = 2\int_0^\infty \mathrm{d}\omega(\alpha^2F(\omega)/\omega)$ and $\omega_{\log} = \exp[(2/\lambda)\int_0^\infty \mathrm{d}\omega(\alpha^2F(\omega)\log(\omega)/\omega)]$.

The superconducting critical temperature T_c is determined using the Allen–Dynes modified McMillan equation [53]

$$T_c = \frac{f_1 f_2 \omega_{\log}}{1.2} \exp\Big[-\frac{1.04(1+\lambda)}{\lambda - \mu^*(1+0.62\lambda)}\Big], \quad (4)$$

where μ^* denotes the Coulomb pseudopotential. f_1, f_2 are functions of λ, μ^* and $\alpha^2F(\omega)$. T_c is also determined by solving the isotropic Migdal–Eliashberg equation, [54] once $\alpha^2F(\omega)$ is obtained.

First-principles calculations were performed using the Quantum ESPRESSO (QE) software package. [76] We employ ultrasoft pseudopotentials with the Perdew–Burke–Ernzerhof (PBE) parametrization [77] of the exchange-correlation potential. The cutoff energies for the wave functions and density were set to 80 Ry and 800 Ry, respectively. Integration over the Brillouin zone in the self-consistent calculations was carried out using Methfessel–Paxton smearing with a broadening of 0.01 Ry and a $21 \times 21 \times 14$ $\boldsymbol{k}$-point grid. Harmonic phonon calculations were performed on a $6 \times 6 \times 3$ $\boldsymbol{q}$-point grid using DFPT. [71] The SSCHA calculations were conducted on a $2 \times 2 \times 1$ supercell, and the resulting anharmonic dynamic matrices were interpolated to a finer $6 \times 6 \times 3$ grid. The electron-phonon interaction was evaluated in both the harmonic and anharmonic cases with a Gaussian smearing of 0.028 Ry. More calculation parameters are listed in the Supplementary Materials.

3. Results and Discussions. The structure of $P6_3/mmc$-SnH_4 is shown in Fig. 1(a) (primitive cell) and Fig. 1(b) ($2\times2\times1$ expansion of the primitive cell). The Sn atoms form a hexagonal close-packed structure, with each Sn atom surrounded by 14 hydrogen atoms. The hydrogen atoms can be divided into two distinct types, which are denoted by H1 and H2 and displayed in different colors in the figure. In the z direction, the H1 atoms lie along the lines passing through the gaps in the Sn sublattice, whereas the H2 atoms lie along the lines intersecting the Sn atoms. In addition, H1 atoms reside on the edges of the primitive cell. We first examine the structural correction arising from quantum ionic vibrations. At fixed pressures ranging from 150 to 240 GPa, we relaxed the crystal structure using SSCHA iteration. The quantum and anharmonic nature of the ions enhances the mechanical stiffness of the crystal, resulting in a ∼1% larger equilibrium unit-cell volume compared with classical harmonic calculations, as shown in Fig. 1(c). The minimum H–H distance, $d_{\mathrm{HH}}^{\min}$ (i.e., the nearest H1 atomic separation), is also increased by the quantum and anharmonic effects, as shown in Fig. 1(d). It should be noted that the nearest H distances of 0.81–0.83 Å are only marginally larger than the H–H bond length (0.766 Å) in compressed solid hydrogen. [78] Such H_2 units are prevalent in tin hydrides. [28,30]

The phonon spectra at four pressures in the range of 150–240 GPa are shown in Fig. 2. As the pressure increases, a moderate overall hardening of the phonon modes can be observed. The phonon modes can be classified into

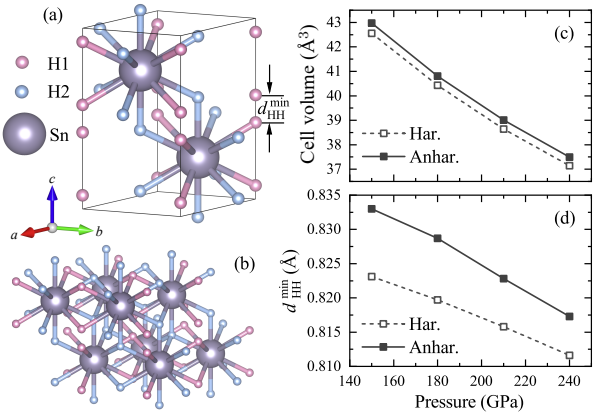

Fig. 1. Crystal structure of SnH_4 in the $P6_3/mmc$ phase, with (a) the primitive cell and (b) a $2\times2\times1$ expansion of the primitive cell. Pressure dependence of (c) the cell volume and (d) the closest distance between hydrogen atoms, calculated both with harmonic approximation (dashed line and hollow symbols), and SSCHA (solid line and symbols) to incorporate the quantum and anharmonic effects.

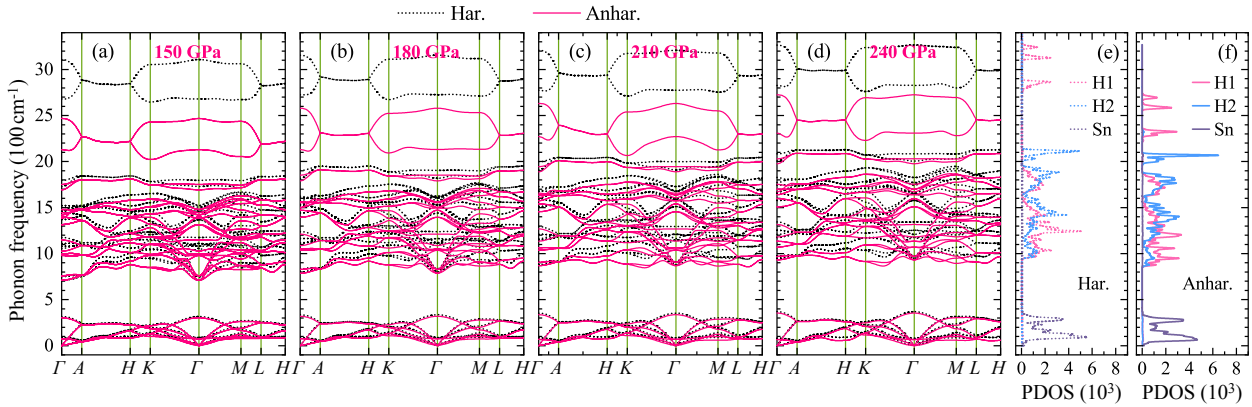

Fig. 2. Comparison of the harmonic (dotted lines) and anharmonic (solid lines) phonon spectra of $P6_3/mmc$-SnH_4 at (a) 150, (b) 180, (c) 210, and (d) 240 GPa. The projected phonon density of states (PDOS) onto each type of atom at 240 GPa are presented, both for the (e) harmonic and (f) anharmonic cases. The unit of PDOS is Ry^{-1}.

three regions based on their frequency magnitudes: low-frequency (less than ∼500 cm^{-1}), mid-frequency (from 500 to ∼2000 cm^{-1}), and high-frequency (above ∼2000 cm^{-1}) regions. Harmonic calculations reveal strict separation among these regions throughout the pressure range. However, incorporating the quantum and anharmonic effects of the ions induces drastic softening of high-frequency optical phonons, exhibiting a 500–600 cm^{-1} downward frequency shift. The mid-energy modes are also shifted slightly downwards by these corrections, whereas the low-energy acoustic phonons remain almost unaffected. Projected phonon density of states (PDOS) for different atoms at 240 GPa are shown in Fig. 2(e) (harmonic approximation) and Fig. 2(f) (including the quantum and anharmonic effects), indicating that heavy Sn atoms dominate the acoustic phonon spectrum, while light H atoms contribute predominantly to the mid-frequency phonon modes. High-frequency optical phonons originate primarily from H1 atoms, indicating site-specific vibrational behavior in this high-pressure phase. The large mass of Sn atoms significantly attenuates quantum nuclear effects and preserves harmonic phonon character. Conversely, hydrogen sublattice vibrations exhibit substantial sensitivity to quantum corrections, with the H1 subsystem exhibiting pronounced anharmonic renormalization.

The superconducting properties were calculated using two frameworks: (1) the harmonic approximation, yielding harmonic T_c; and (2) the SSCHA incorporating quantum anharmonic effects, yielding the anharmonic T_c. The anharmonic electron–phonon coupling matrices were computed using the SSCHA free-energy Hessian phonons. Critical temperatures were computed using the Allen–Dynes modified McMillan (AD) equation and by solving isotropic Migdal–Eliashberg (ME) equations. Figure 3(a) displays the pressure dependence of T_c using the AD equation, while Fig. 3(b) shows equivalent results from ME solutions.

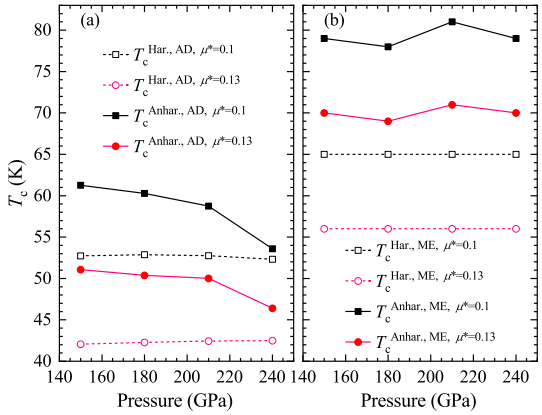

Fig. 3. The calculated T_c for $P6_3/mmc$-SnH_4 in the pressure range of 150–240 GPa, both with harmonic approximation (denoted by dashed lines and hollow symbols) and SSCHA (denoted by solid lines and symbols). (a) Results computed from the Allen–Dynes (AD) equation. (b) Results obtained by solving the isotropic Migdal–Eliashberg (ME) equations. The Coulomb pseudopotential μ^* is set as values of 0.1 (black) and 0.13 (red).

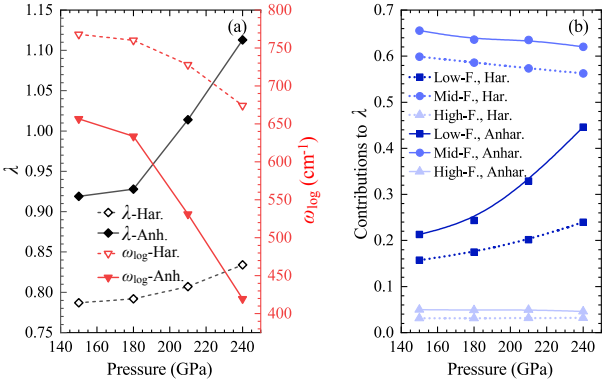

Fig. 4. (a) Pressure dependence of the electron–phonon coupling constant λ (black) and average logarithmic frequency ω_{log} (red), calculated with both the harmonic approximation (denoted by dashed lines and hollow symbols) and SSCHA (denoted by solid lines and symbols). (b) Pressure dependence of contributions to λ from low- (<500 cm^{-1}), mid- (500–∼2000 cm^{-1}), and high-frequency (>∼2000 cm^{-1}) phonons.

Using the AD equation at $\mu^* = 0.1$, the harmonic T_c remains nearly pressure-independent at ∼53 K across the 150–240 GPa. Increasing μ^* to 0.13 reduces T_c to ∼42 K. Incorporating quantum and anharmonic corrections increases T_c to ∼61 K at 150 GPa ($\mu^* = 0.1$) but induces a progressive decline to ∼54 K at 240 GPa, in sharp contrast to the harmonic trend. To elucidate this pressure dependence, we present the electron–phonon coupling constant λ and average logarithmic frequency ω_{log} in Fig. 4(a). With the harmonic approximation, whereas the gradual increase of λ from 0.79 (150 GPa) to 0.83 (240 GPa) would normally enhance T_c, this effect is counterbalanced by the simultaneous decrease in ω_{log} from 770 cm^{-1} to 670 cm^{-1}, yielding a net pressure-insensitive harmonic T_c. Quantum and anharmonic effects amplify both trends: that is, λ increases markedly and ω_{log} decreases rapidly, collectively driving the anharmonic T_c reduction with pressure. Our result of harmonic T_c from the AD equation is approximately 10 K lower than that predicted by Gao *et al.* in 2010.[29] This T_c discrepancy mainly stems from the deviation of $\lambda = 0.81$ here at ∼200 GPa from their value of 0.87. Further examination attributes the λ deviation to distinct contributions from the mid-frequency phonon modes.

The solutions of the ME equations [Fig. 3(b)] significantly exceed the predictions from the AD equation: the harmonic T_c at $\mu^* = 0.1$ ($\mu^* = 0.13$) is elevated to a pressure-independent value of 65 K (56 K), and the anharmonic T_c at $\mu^* = 0.1$ ($\mu^* = 0.13$) increases to 79 K (70 K) with a slight oscillation with pressure. These results demonstrate that the quantum and anharmonic effects substantially enhance T_c in stannane, as in the case of $LaBH_8$,[42] which contrasts sharply with the suppressive effects in many other hydride superconductors.[37,79,80] In addition, our anharmonic T_c of ∼70 K from ME equations at $\mu^* = 0.13$ is numerically close to the measured T_c of 70–72 K in recent experiments on tin hydrides.[32,33] However, the similar X-ray diffraction spectra in these two experiments are identified as two significantly distinct phases of

$C2/m$-SnH_{12} and $Fd\bar{3}m$-Sn_8H_{30}, indicating that significant uncertainty still persists regarding structural assignment of the observed samples.

To further analyze the atomic origin of the superconducting behavior, we decomposed λ into components from three phonon frequency regimes: low-frequency (less than 500 cm^{-1}), mid-frequency (from 500 to ~2000 cm^{-1}), and high-frequency (above ~2000 cm^{-1}). As shown in Fig. 4(b), mid-frequency phonons, which primarily arise from both H1 and H2 hydrogen vibrations, dominate λ contributions (60%–70%), though their share decreases with increasing pressure. On the other hand, the low-frequency acoustic modes, whose PDOS are dominated by Sn atomic motions, contribute 20%–40% with progressively increasing pressure dependence, thereby driving the increase of total λ with pressure. A minor residual contribution (~5%) from the high-frequency optical phonons originates exclusively from H1 atoms. Crucially, quantum and anharmonic corrections predominantly enhance the low- and mid-frequency phonon contributions. The Eliashberg spectral function $\alpha^2F(\omega)$ and its frequency-rescaled integral $\lambda(\omega) = \int_0^\omega 2(\alpha^2F(\omega')/\omega')\mathrm{d}\omega'$ at 210 GPa are shown in Figs. 5(a2) and 5(b2), for the harmonic and anharmonic cases, respectively. The projected $\alpha^2F(\omega)$ onto H1, H2 and Sn can be obtained by calculating the partial diagonal contributions from different types of atoms of the phonon linewidth $\gamma_\mu(\boldsymbol{q})$ in Eq. (3), and are displayed in Figs. 5(a3)–5(a5) (harmonic) and Figs. 5(b3)–5(b5) (anharmonic). Note that the the sum of the partial $\alpha^2F(\omega)$ from all three types of atoms is not the total $\alpha^2F(\omega)$, because there are off-diagonal components of $\alpha^2F(\omega)$, in addition to the diagonal components. The corresponding PDOS of phonons are shown in Figs. 5(a1) and 5(b1) for comparison. The data at other pressures are shown in the Supplementary Materials. Figure 5 shows that while Sn-derived phonon modes exhibit substantial density of states,

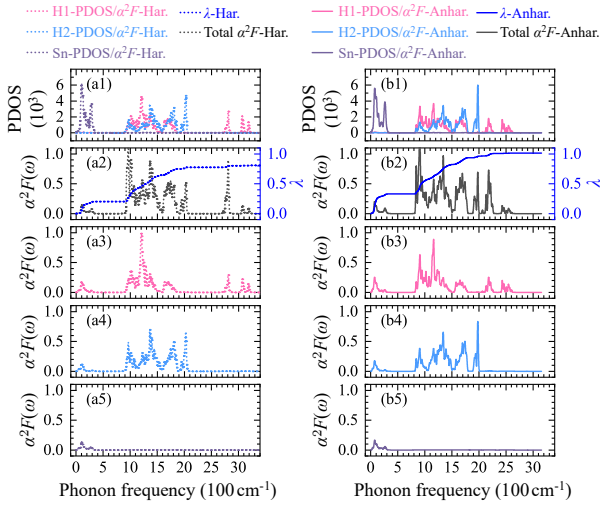

Fig. 5. (a1) and (b1) The projected phonon density of states (PDOS) onto each type of atom at 210 GPa. (a2) and (b2) The Eliashberg spectral function $\alpha^2F(\omega)$ (black) and its frequency-rescaled integral (blue). The projected $\alpha^2F(\omega)$ onto (a3) and (b3) H1, (a4) and (b4) H2, and (a5) and (b5) Sn atoms. The dotted lines denote results obtained with the harmonic approximation, while the solid lines correspond to the SSCHA calculations.

their contribution to the Eliashberg function $\alpha^2F(\omega)$ remains relatively low. By contrast, hydrogen atoms, despite having negligible density of states in low-frequency acoustic modes, contribute significantly to $\alpha^2F(\omega)$ compared to Sn. With harmonic approximation, the λ-components of the acoustic and optical phonon modes at 210 GPa are 0.20 and 0.61, respectively, and the quantum and anharmonic corrections increase them to 0.33 and 0.68, respectively. This demonstrates a stronger reinforcement of the acoustic-mode coupling than optical-mode coupling under quantum and anharmonic corrections.

4. Summary. To summarize, we investigated the quantum and anharmonic corrections of vibrational ions to determine the structural and superconducting properties of SnH_4 in $P6_3/mmc$ phase within the 150–240 GPa pressure range, using DFT calculations combined with SSCHA. Compared with calculations based on the classical harmonic approximation, inclusion of quantum ionic effects enhances the mechanical stiffness of the lattice, expanding the cell volume by ~1% at fixed pressures. These corrections substantially soften the optical phonon modes derived from hydrogen vibrations, with particularly pronounced shifts of approximately 500–600 cm^{-1} downward for the high-frequency modes exceeding 2000 cm^{-1}. This demonstrates the importance of the quantum motion of light hydrogen atoms. The superconducting critical temperature T_c was computed based on the harmonic and anharmonic phonon spectra, via the Allen–Dynes modified McMillan formulism and isotropic Migdal–Eliashberg equations. Harmonic approximation yields pressure-independent T_c of 53 K (from Allen–Dynes) and 65 K (from Migdal–Eliashberg) within 150–240 GPa, with μ^* set to 0.1. The quantum and anharmonic corrections increase T_c to ~61 K at 150 GPa ($\mu^* = 0.1$) but induce progressive decrease to ~54 K at 240 GPa using the Allen–Dynes equation. For Migdal–Eliashberg predictions, these effects increase T_c to ~79 K ($\mu^* = 0.1$). At $\mu^* = 0.13$, anharmonic T_c of ~70 K from Migdal–Eliashberg equations is close to the value of 70–72 K measured in recent experiments on tin binary hydrides,[32,33] whereas the specific structures of the synthesized samples are still in controversy. Furthermore, the electron–phonon coupling constant λ, Eliashberg spectral function $\alpha^2F(\omega)$, and their components were analyzed. The results indicate that quantum and anharmonic corrections predominantly amplify the $\alpha^2F(\omega)$ components from low-frequency acoustic modes. While these modes mainly originate from the Sn atoms, the small subset derived from hydrogen atoms contributes disproportionately to $\alpha^2F(\omega)$, resulting in a sensitive hydrogen-originated response of acoustic modes to quantum ionic effects. This work enriches the dataset for tin hydrides and provides insights into superconducting mechanisms in high-pressure hydrides.

Acknowledgements. This work was supported by the Scientific Research Program Funded by Shaanxi Provincial Education Department (Grant No. 24JP126), the National Natural Science Foundation of China (Grant No. 62174136), and the Natural Science Basic Research Program of Shaanxi Province (Grant No. 2025JC-YBMS-063).

References

[1] Gor'kov L P and Kresin V Z 2018 *Rev. Mod. Phys.* **90** 011001
[2] Sun W, Kuang X, Keen H D J, Lu C, and Hermann A 2020 *Phys. Rev. B* **102** 144524
[3] Flores-Livas J A, Boeri L, Sanna A, Profeta G, Arita R, and Eremets M 2020 *Phys. Rep.* **856** 1
[4] Kong P, Minkov V S, Kuzovnikov M A *et al.* 2021 *Nat. Commun.* **12** 5075
[5] Chen B, Conway L J, Sun W, Kuang X, Lu C, and Hermann A 2021 *Phys. Rev. B* **103** 035131
[6] Zhang Z, Cui T, Hutcheon M J, Shipley A M, Song H, Du M, Kresin V Z, Duan D, Pickard C J, and Yao Y 2022 *Phys. Rev. Lett.* **128** 047001
[7] Minkov V, Bud'ko S, Balakirev F, Prakapenka V, Chariton S, Husband R, Liermann H, and Eremets M 2022 *Nat. Commun.* **13** 3194
[8] Zhao W, Huang X, Zhang Z, Chen S, Du M, Duan D, and Cui T 2023 *Natl. Sci. Rev.* **11** nwad307
[9] Sun Y, Zhong X, Liu H, and Ma Y 2024 *Natl. Sci. Rev.* **11** nwad270
[10] Eremets M I 2024 *Natl. Sci. Rev.* **11** nwae047
[11] Cerqueira T F, Fang Y W, Errea I, Sanna A, and Marques M A 2024 *Adv. Funct. Mater.* **34** 2404043
[12] Fang Y W, Dangić D, and Errea I 2024 *Commun. Mater.* **5** 61
[13] Sanna A, Cerqueira T F, Fang Y W, Errea I, Ludwig A, and Marques M A 2024 *npj Comput. Mater.* **10** 44
[14] He X L, Zhao W, Xie Y, Hermann A, Hemley R J, Liu H, and Ma Y 2024 *Proc. Natl. Acad. Sci. U.S.A.* **121** e2401840121
[15] Li Z, He X, Zhang C, Lu K, Zhang J, Zhang S, Zhao J, Shi L, Peng Y, Feng S, Deng Z, Liu Q, Wang X, Wang L, Prakapenka V, Chariton S, Liu H, and Jin C 2025 *Chin. Phys. Lett.* **42** 047401
[16] Deng C, Wang M, Guo S, Huang H, Du M, Duan D, Song H, and Cui T 2025 *Chin. Phys. Lett.* **42** 070711
[17] Li B, Cao Z, Zhai J, Wu M, Chi D, Liu S, and Sun J 2026 *Chin. Phys. Lett.* **43** 010712
[18] Lu W, Hutcheon M J, Hansen M F, Dolui K, Sinha S, Sahoo M R, Pickard C J, Heil C, Pakhomova A, Mezouar M, Daisenberger D, Chariton S, Prakapenka V, Julian M N, Prasankumar R P, and Strobel T A 2025 *Phys. Rev. B* **112** 094513
[19] Li S A, Niu R, Liu Y M, Fu X, Chen X J, Lin H Q, and Zhong G H 2025 *Phys. Rev. B* **111** 054523
[20] Ma Y, Luo J, Meng S, Zhong X, Liu G, Liu H, and Ma Y 2025 *Phys. Rev. B* **111** 184512
[21] Semenok D V, Altshuler B L, and Yuzbashyan E A 2025 *Adv. Mater.* **37** 2507013
[22] Sato R, Conway L J, Zhang D, Pickard C J, Akagi K, Sau K, Li H, and Orimo S 2025 *Proc. Natl. Acad. Sci. U.S.A.* **122** e2413480122
[23] Gao K, Cerqueira T F, Sanna A, Fang Y W, Dangić D, Errea I, Wang H C, Botti S, and Marques M A 2025 *Nat. Commun.* **16** 8253
[24] Ashcroft N W 1968 *Phys. Rev. Lett.* **21** 1748
[25] Ashcroft N 2004 *Phys. Rev. Lett.* **92** 187002
[26] Drozdov A, Eremets M, Troyan I, Ksenofontov V, and Shylin S I 2015 *Nature* **525** 73
[27] Somayazulu M, Ahart M, Mishra A K, Geballe Z M, Baldini M, Meng Y, Struzhkin V V, and Hemley R J 2019 *Phys. Rev. Lett.* **122** 027001
[28] Tse J S, Yao Y, and Tanaka K 2007 *Phys. Rev. Lett.* **98** 117004
[29] Gao G, Oganov A R, Li P, Li Z, Wang H, Cui T, Ma Y, Bergara A, Lyakhov A O, Iitaka T, and Zou G 2010 *Proc. Natl. Acad. Sci. U.S.A.* **107** 1317
[30] Zhang H, Jin X, Lv Y, Zhuang Q, Li Y, Bao K, Li D, Liu B, and Cui T 2016 *RSC Advances* **6** 10456
[31] Mahdi Davari Esfahani M, Wang Z, Oganov A R, Dong H, Zhu Q, Wang S, Rakitin M S, and Zhou X F 2016 *Sci. Rep.* **6** 22873
[32] Hong F, Shan P, Yang L *et al.* 2022 *Mater. Today Phys.* **22** 100596
[33] Troyan I A, Semenok D V, Ivanova A G *et al.* 2023 *Adv. Sci.* **10** 2303622
[34] Errea I, Belli F, Monacelli L *et al.* 2020 *Nature* **578** 66
[35] Borinaga M, Errea I, Calandra M, Mauri F, and Bergara A 2016 *Phys. Rev. B* **93** 174308
[36] Bianco R, Errea I, Calandra M, and Mauri F 2018 *Phys. Rev. B* **97** 214101
[37] Hou P, Belli F, Bianco R, and Errea I 2021 *Phys. Rev. B* **103** 134305
[38] Monacelli L, Bianco R, Cherubini M, Calandra M, Errea I, and Mauri F 2021 *J. Phys.: Condensed Matter* **33** 363001
[39] Belli F 2022 *Characterization of hydrogen based superconductors from first principles* Ph.D. thesis, University of the Basque Country
[40] Bianco R, Errea I, Paulatto L, Calandra M, and Mauri F 2017 *Phys. Rev. B* **96** 014111
[41] Ribeiro G A S, Paulatto L, Bianco R, Errea I, Mauri F, and Calandra M 2018 *Phys. Rev. B* **97** 014306
[42] Belli F and Errea I 2022 *Phys. Rev. B* **106** 134509
[43] Dangić D, Fang Y W, Cerqueira T F, Sanna A, Novoa T, Gao H, Marques M A, and Errea I 2025 *Comput. Mater. Today* **8** 100043
[44] Dong G, Cui T, Huo Z, Liu Z, Chen W, Hou P, Fang Y W, and Duan D 2025 *Mater. Today Phys.* **59** 101939
[45] Ding Y, Chen H, and Shi J 2025 *Phys. Rev. B* **112** 184517
[46] Wan Z, Zhong G H, Zhang R, and Lin H Q 2025 *Phys. Rev. B* **112** L220504
[47] Errea I, Calandra M, and Mauri F 2014 *Phys. Rev. B* **89** 064302
[48] Monacelli L, Errea I, Calandra M, and Mauri F 2018 *Phys. Rev. B* **98** 024106
[49] Monacelli L and Mauri F 2021 *Phys. Rev. B* **103** 104305
[50] Cooper L N, Bardeen J, and Schrieffer J 1957 *Phys. Rev* **108** 1175
[51] Migdal A 1958 *Sov. Phys. JETP* **7** 996
[52] Eliashberg G 1960 *Sov. Phys. JETP* **11** 696
[53] Allen P B and Dynes R C 1975 *Phys. Rev. B* **12** 905
[54] Allen P B and Mitrović B 1983 *Solid State Physics* **37** 1
[55] Duan D, Huang X, Tian F, Li D, Yu H, Liu Y, Ma Y, Liu B, and Cui T 2015 *Phys. Rev. B* **91** 180502
[56] Peng F, Sun Y, Pickard C J, Needs R J, Wu Q, and Ma Y 2017 *Phys. Rev. Lett.* **119** 107001
[57] Kim D Y, Scheicher R H, Pickard C J, Needs R, and Ahuja R 2011 *Phys. Rev. Lett.* **107** 117002
[58] Liu H, Li Y, Gao G, Tse J S, and Naumov I I 2016 *J. Phys. Chem. C* **120** 3458
[59] Li Y, Hao J, Liu H, Tse J S, Wang Y, and Ma Y 2015 *Sci. Rep.* **5** 9948
[60] Zhong X, Wang H, Zhang J, Liu H, Zhang S, Song H F, Yang G, Zhang L, and Ma Y 2016 *Phys. Rev. Lett.* **116** 057002
[61] Liang X, Zhao S, Shao C *et al.* 2019 *Phys. Rev. B* **100** 184502
[62] Liang X, Bergara A, Wang L, Wen B, Zhao Z, Zhou X F, He J, Gao G, and Tian Y 2019 *Phys. Rev. B* **99** 100505
[63] Zhang P, Sun Y, Li X, Lv J, and Liu H 2020 *Phys. Rev. B* **102** 184103
[64] Jiang M J, Hai Y L, Tian H L, Ding H B, Feng Y J, Yang C L, Chen X J, and Zhong G H 2022 *Phys. Rev. B* **105** 104511
[65] Zhao W, Duan D, Du M, Yao X, Huo Z, Jiang Q, and Cui T 2022 *Phys. Rev. B* **106** 014521

[66] Du M, Li Z, Duan D, and Cui T 2023 *Phys. Rev. B* **108** 174507
[67] Yang K, Cui W, Hao J, Shi J, and Li Y 2023 *Phys. Rev. B* **107** 024501
[68] Shi L T, Si J G, Turnbull R, Liang A, Liu P F, and Wang B T 2024 *Phys. Rev. B* **109** 054512
[69] Chen W, Ma T, Huo Z, Yu H, Cui T, and Duan D 2024 *Phys. Rev. B* **109** 224505
[70] Liu S Y, Huo P Y, Jiang W Z, Yang R Y, and Liu Y H 2024 *Phys. Rev. B* **109** 104514
[71] Baroni S, de Gironcoli S, Dal Corso A, and Giannozzi P 2001 *Rev. Mod. Phys.* **73** 515
[72] Setty C, Baggioli M, and Zaccone A 2020 *Phys. Rev. B* **102** 174506
[73] Setty C, Baggioli M, and Zaccone A 2021 *Phys. Rev. B* **103** 094519
[74] Zacharias M, Volonakis G, Giustino F, and Even J 2023 *Phys. Rev. B* **108** 035155
[75] Lihm J M and Park C H 2021 *Phys. Rev. Res.* **3** L032017
[76] Giannozzi P, Baroni S, Bonini N *et al.* 2009 *J. Phys.: Condensed matter* **21** 395502
[77] Perdew J P, Burke K, and Ernzerhof M 1996 *Phys. Rev. Lett.* **77** 3865
[78] Pickard C J and Needs R J 2007 *Nat. Phys.* **3** 473
[79] Ma Y, Li M, Shi W, Wang V, Hou P, and Pang M 2024 *Chin. Phys. Lett.* **41** 127402
[80] Hou P, Ma Y, Pang M, Cai Y, Shen Y, Xie H, and Tian F 2024 *J. Chem. Phys.* **161** 024504